Assessing Synchrophasor Estimates of an Event Captured by a Phasor Measurement Unit

José Antonio de la O Serna, *Senior Member, IEEE,* Mario R. Arrieta Paternina, *Member, IEEE,* and Alejandro Zamora-Mendez, *Member, IEEE*

***Abstract*—Synchrophasor estimators are nowadays evaluated with the Total Vector Error (TVE) using the synchrophasor representations of the few benchmark signals. This synchrophasor dependence prevents its application to power signals of real events. A new method to obtain the synchrophasor of real signals is proposed in this paper. A finite impulse response (FIR) filter, designed with the nonic O-spline is proposed to obtain phasor estimates asymptotically close to those of an ideal bandpass filter. The phasor estimation accuracy of one or several Phasor Measurement Units (PMUs) can be then assessed using the standard. In addition, it is possible to design two FIR differentiators to obtain frequency and ROCOF estimates close enough to those of ideal differentiator filters, and largely compliant with the standard. This new set of filters opens the way to apply the synchrophasor standard to assess estimates of PMUs of different brands when they process the same signals of a power system event. In this paper, the erratic phasor and frequency estimates produced by a SEL-351A PMU from a real distributed generation system are assessed to corroborate that the synchrophasor standard can be opened to this new application based on real signals from the field, previously considered as impossible.**

***Index Terms*—Frequency, O-splines, phasor measurement unit, rate of change of frequency, synchrophasors, total vector error.**

I. Introduction

DYNAMIC synchrophasor estimation from power system signals continues being an open problem and a challenge to improve the performance of power systems in general, and of modern grids with renewable energy resources in particular. As the Wide-Area Monitoring System (WAMS) [1] installations are growing, phasor data are taken into account to support the decision process needed to increase the reliability of power grids.

Recently, phasor measurement technology and synchrophasor networks have expanded significantly in many countries [2]-[6]. In the meantime, a considerable effort is done to regulate the required parameter accuracy [7]. However, there are still cases in which erratic estimates or coarse parameters are furnished by devices as the one disclosed in this paper. This indicates that those earnest efforts to foster instrumentation are failing in tailoring it to its high-fidelity demands.

J. A. de la O Serna is with the Department of Electrical Engineering, Autonomous University of Nuevo León, Monterrey, NL 66450, Mexico (e-mail: jdelao@ieee.org).

M. Arrieta Paternina is with the Department of Electrical Engineering, National Autonomous University of Mexico, Mexico City 04510, Mexico, (e-mail: mra.paternina@fi-b.unam.mx).

A. Zamora-Mendez is with Electrical Engineering Faculty, Universidad Michoacana de San Nicolas de Hidalgo, Morelia, Mich. 58030, Mexico (e-mail: azamoram@umich.mx).

Despite the concept of dynamic phasor [8] is now adopted in the recent International Standard of Synchrophasors for Power Systems [9], its estimation error is still the Total Vector Error (TVE) defined in [10]-[11]. TVE was conceived to combine amplitude and phase errors into a single measure [12]. But its definition assumes steady-state signals during the observation window, which is valid only for static phasors, but clearly insufficient for dynamic ones. In addition, TVE is useful only for signals whose synchrophasors are known.

Algorithms based on the Discrete Fourier Transform (DFT) [13]-[16] are designed under the TVE static assumption. Presumption of signals with dynamic amplitude and phase variations, leads to new methods such as those in [17]-[19], and has impelled the successive amendments of the Standard for Synchrophasor Measurements for Power Systems [10]-[11].

Nowadays, the focus of the standard is placed on the noise sensitivity of the PMUs [20], on frequency and Rate of Change of Frequency (ROCOF) estimation problems [21]-[23]. But evidence of this paper indicates that an effort is still needed to improve the basic accuracy of PMU technology.

Synchrophasor standard [9]-[11] defines a dynamic synchrophasor representation for power system signals and its measurement requirements. It establishes static and dynamic requests, including those for transient performance. Its benchmark signals are crucial since they constitute the only measurands for TVE. Nonetheless, they establish also its main weakness, since TVE and the synchrophasor standard itself is useless to assess PMU estimates obtained from real signals, for which their synchrophasors are not available.

Our research problem is an event captured by a SEL-351A PMU. It was recorded in a small system with a distributed solar and wind power generation. The PMU provided its own phasor estimates and the oscillographic data of voltages and currents. Under this circumstances, our problem consists in assessing the rendered PMU phasor estimates, or those obtained with any other phasor estimation algorithm. But TVE cannot be applied in this case, since the ideal synchrophasors of the real signals of the event are not available. This is a Kuhn's anomaly for the Standard. To solve it, we need a method to obtain the ideal synchrophasors of the real signals.

At that time, FIR filters designed with O-splines were numerically available [17], and we thought that synchrophasors from the event could be obtained with one of those filters with high order. The O-splines were found recently in closed-form in [24], and disclosed as convergent to the ideal lowpass filter, when the order K goes to ∞. In consequence, they provide a

Cauchy sequence of filters that perform as ideal filters as the order increases. This means that if the signal spectral density about the fundamental frequency is contained under their ideal gain, its phasor estimates also converge to the ideal one: i. e., the synchrophasor we need to obtain.

The contribution of this paper is to propose a convergent series of bandpass FIR filters designed with O-splines to obtain phasor estimates sufficiently closed to the ideal synchrophasors of signals coming from the field. There is not a single published paper attempting to assess the PMU performance from real signals, most of them are done with test systems [25] or real time digital simulators [26]. All of them are about the Standard benchmark signals, whose main shortcoming is precisely that it depends on known synchrophasors.

For the signals of the event, we observed that the Euclidean distance between phasor estimates obtained with the nonic and decimononic filters are already very small. For a Cauchy sequence, this means that the nonic estimates are already very close to the ideal ones. In consequence, in this paper a FIR filter designed with the nonic O-spline [24] is proposed to obtain the synchrophasor of the real signals. This method not only opens the way to the use of TVE to assess the accuracy of the PMU based on real signals, such as those available in a control center; but also to the application of the whole synchrophasor standard to real signals, which until now it is confined to its benchmark signals. In addition, the provided method provides a very accurate filter for phasor estimation, with smaller errors than those of high-accuracy filters proposed in the recent literature [27], [28], and [29].

Another advantage of the O-splines is that with its first two derivatives it is possible to design FIR differentiators to estimate frequency and ROCOF with high accuracy. They also converge to ideal bandpass differentiators.

The remainder of the paper is organized as follows. Section II compares the frequency response of the Cosine filter with the nonic FIR filter, and presents its two first differentiators. The rationale of the proposed method for obtaining the synchrophasors from real signals is presented in Section III. In Section IV, we show that the proposed filters are compliant with the standard. Then, the topology of the system of the recorded event, the oscillographic data, and the estimates provided by the PMU are presented in Section V. Section VI presents the obtained synchrophasors and the TVE of the PMU estimates, as well as the PMU frequency estimates. It is concluded that PMU estimates are awfully erratic, not only in phase but also in amplitude.

II. Compared filters

In this section, the formulation of the compared filters is developed and their frequency responses illustrated. The Cosine filter is implemented in the PMU that furnished the analyzed data. And the nonic O-spline provide the high-order FIR filter with which we obtain the best synchrophasor estimates from the given signals.

A. Cosine filter

The formulation of the implemented *Cosine* filter, is taken from [30]. It is a "mimic" version of the full-cycle Fourier filter, whose phasor estimate at ℓ, ξ_ℓ, is given by [31]:

$$\widehat{\xi}_\ell = \langle x_\ell, \frac{1}{N} e^{j\theta_1 n} \rangle = \frac{1}{N} \sum_{n=-\frac{N}{2}}^{\frac{N}{2}-1} x(\ell+n) e^{-j\theta_1 n}, \quad (1)$$

where x_ℓ is a vector with last available signal segment of one-cycle, $\frac{1}{N} e^{j\theta_1 n}$ is another vector with that sequence, and $\theta_1 = \frac{2\pi}{N}$ is the angular fundamental frequency.

The *Cosine* filter projects a complex signal $x_\ell + j x_{\ell-N/4}$ onto the real part of the complex exponential function. We have:

$$\widehat{c}_\ell = \mathrm{Re}\{\widehat{\xi}_{c\ell}\} = \langle x_\ell, \frac{1}{N} \cos\theta_1 n \rangle \quad (2)$$

$$\widehat{c}_{\ell-N/4} = \mathrm{Im}\{\widehat{\xi}_{c\ell}\} = \langle x_{\ell-N/4}, \frac{1}{N} \cos\theta_1 n \rangle \quad (3)$$

Its complex form illustrates the key idea of the *Cosine* filter:

$$\widehat{\xi}^c_\ell = \widehat{c}_\ell + j\widehat{c}_{\ell-N/4} = \langle x_\ell + j x_{\ell-N/4}, \frac{1}{N} \cos(\theta_1 n) \rangle. \quad (4)$$

Notice that the anti-rotation of a quarter cycle in the sequence $x_{\ell-N/4}$ is compensated by the factor j of the imaginary part.

Of course, this construction assumes that the analyzed signal frequency is equal to the fundamental and that amplitude and phase must be constant during one and a quarter of a cycle. This supposition constitutes the main weakness of this phasor estimator, especially when the power signal is oscillating.

According to (1), from a signal of length L a sequence of phasor estimates $\widehat{\xi}^c_\ell, \ell = \frac{N}{2}, \frac{N}{2}+1, \ldots, L-\frac{N}{2}+1$, can be obtained as follows:

$$\widehat{\xi}^c_\ell = \frac{1}{N} \sum_{n=-\frac{N}{2}}^{\frac{N}{2}-1} [x_{\ell+n} + j x_{\ell-\frac{N}{4}+n}] \cos\theta_1 n, \quad (5)$$

with the following z transform [31], [32]:

$$\Xi^c(z) = X(z) z^\ell [1 + j z^{-N/4}] \frac{1}{N} \sum_{n=0}^{N-1} \cos(\theta_1 n) z^{-n}, \quad (6)$$

thus, after the anti-rotation ($z^{-\ell}$), the transfer function of the Cosine filter, is

$$H^c(z) = [1 + j z^{-N/4}] H_c(z), \quad (7)$$

and $H^c(e^{j\theta})$ is its frequency response in terms of the angular frequency θ, for $-\pi \le \theta \le \pi$. Fig. 1 shows the frequency response of the Cosine filter. It is asymmetric, and with high sidelobes that infiltrate the image (negative) fundamental frequency when the signal is under oscillating conditions.

The Cosine filter implemented according to the available literature of the seller [30] provided phasor estimates much less erratic than those of the one implemented in the PMU. We assume that this algorithm is compliant with the Synchrophasor Standard as a P class filter due to its applications in many protection systems. Its compliance with the Standard is beyond the scope of this paper.

This article has been accepted for publication in a future issue of this journal, but has not been fully edited. Content may change prior to final publication. Citation information: DOI 10.1109/TPWRD.2020.3033755, IEEE Transactions on Power Delivery

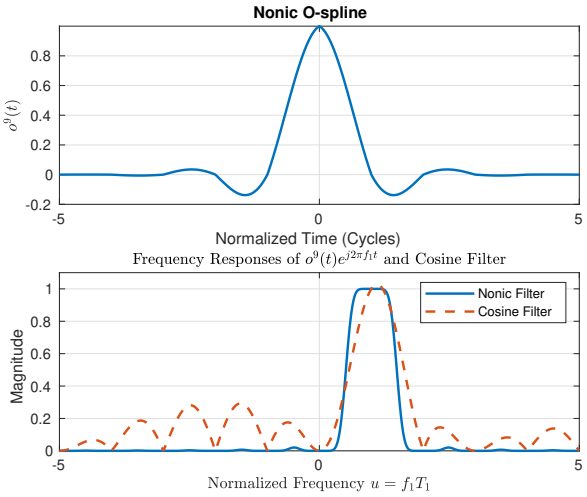

Fig. 1. Ten-cycle Nonic O-spline (top plot), and at the bottom the frequency responses of the nonic bandpass filter used to extract the synchrophasor, and of the Cosine filter used in the PMU.

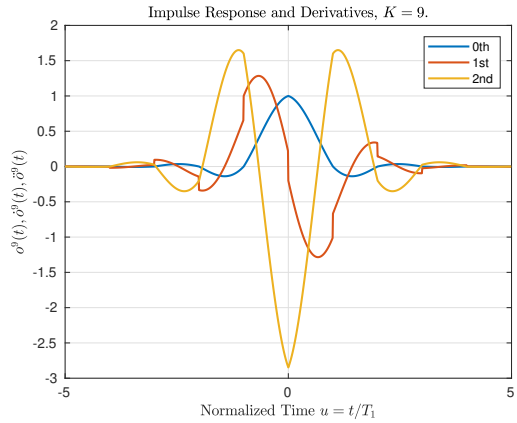

Fig. 2. Impulse Response of nonic Taylor-Fourier Lowpass Filter, and first two derivatives.

B. Nonic O-spline FIR bandpass filter

In [8] the accuracy of DFT phasor estimates was improved under oscillatory conditions, by adding Taylor terms modulated at the fundamental frequency. Then, the DTTFT was proposed in [17] to expand the dynamic phasor estimates to the harmonics included in the sampling frequency band. Finally, it was found that DTTFT bandpass digital filters are simple modulated version of the O-splines, which were found in closed-form in [24].

The polynomial cyclic pieces $p_c(u), c = 1, 2, \ldots, K+1$ of any O-spline of order K can be obtained [24] by the following equation:

$$p_c(u) = \frac{1}{D_c} \prod_{\substack{n=1 \\ n \neq c}}^{K+1} (u + n - c), \quad c = 1, 2, \ldots, K+1 \tag{8}$$

where u is the cyclic time normalized with respect to the fundamental period $u = [0, 1)$, c is the index of the polynomial pieces from left to right, and the common denominator D_c is the product of the roots of each polynomial piece $p_c(u)$. Any odd order K O-spline $\widetilde{\varphi}_0^{(K)}(u)$, $u = [-(K+1)/2, (K+1)/2]$, can be obtained as a simple consecutive concatenation of the polynomial pieces in (8). This analytic formulation circumvents the numerical instability in the inversion of the Taylor matrix found in the algorithm of its numerical solution [17], due to the small determinants of the Taylor matrices when the sampling time is small and K is large. The Matlab function used to calculate O-splines of order K and its first two derivatives can be found in Appendix A.

DTTFT bandpass filters are simply modulated versions of the O-splines at a particular harmonic frequency. We have:

$$h_m^{(K)}(u) = \widetilde{\varphi}_0^{(K)}(u) e^{j2\pi m u}, \quad m = 0, 1, \ldots, M-1. \tag{9}$$

In [24] it is demonstrated that O-splines tend to the ideal lowpass filter as the order $K \to \infty$, and that their derivatives tend to the corresponding ideal differentiator. Then the synchrophasor of a real signal can be extracted with $h_1^{(K)}(u)$ and an order K sufficiently large.

The top plot of Fig. 1 shows the nonic O-spline $\widetilde{\varphi}_0^{(9)}(t)$ with a duration of ten cycles, and the bottom plot depicts the frequency response of the nonic DTTFT bandpass filter $h_1^{(K)} = \widetilde{\varphi}_0^{(9)}(t) e^{j2\pi f_1 t}$ at the nominal fundamental frequency f_1, used in this paper to extract the synchrophasor of voltage and current signals of the event. Despite its support of ten cycles, the two polynomial pieces at its extremes are very small. They can not be truncated since they are very important to shape its spectrum, but the transient of its step response can be considered of only 6 cycles, for practical purposes.

Fig. 2 displays the nonic O-spline and its first two derivatives. By modulating these at the nominal fundamental frequency, we obtain the impulse responses of the bandpass differentiators that estimate the phasor derivatives, from which frequency and rate of change of frequency (ROCOF) are obtained.

The first differentiator modulated at the m-th harmonic is given by:

$$f_m^{(K)}(u) = f_0 \dot{\widetilde{\varphi}}_0^{(K)}(u) e^{j2\pi m u}, \quad m = 0, 1, \ldots, M-1, \tag{10}$$

and the second differentiator by:

$$r_m^{(K)}(u) = f_0^2 \ddot{\widetilde{\varphi}}_0^{(K)}(u) e^{j2\pi m u}, \quad m = 0, 1, \ldots, M-1. \tag{11}$$

where f_0 is the central or fundamental frequency.

The discrete time versions of (9)-(11) is divided by N_0, the number of samples per fundamental cycle. See (7) in [24], and Appendix B.

Amplitude and phase derivatives can be obtained from the estimates of the phasor and its first derivatives, as follows [33]:

$$\widehat{a}_\ell = 2|\widehat{\xi}_\ell| \qquad \widehat{\varphi}_\ell = \measuredangle \widehat{\xi}_\ell \tag{12}$$

$$\dot{\widehat{a}} = 2\,\mathrm{Re}\{\dot{\widehat{\xi}}_\ell e^{-j\widehat{\varphi}_\ell}\} \qquad \dot{\widehat{\varphi}}_\ell = \frac{2}{\widehat{a}_\ell}\,\mathrm{Im}\{\dot{\widehat{\xi}}_\ell e^{-j\widehat{\varphi}_\ell}\} \tag{13}$$

$$\ddot{\widehat{a}}_\ell = 2\,\mathrm{Re}\{\ddot{\widehat{\xi}}_\ell e^{-j\widehat{\varphi}_\ell}\} + \widehat{a}_\ell \dot{\widehat{\varphi}}_\ell^2 \big| \ddot{\widehat{\varphi}}_\ell = \frac{2}{\widehat{a}_\ell}\,\mathrm{Im}\{\ddot{\widehat{\xi}}_\ell e^{-j\widehat{\varphi}_\ell}\} - \dot{\widehat{a}}_\ell \dot{\widehat{\varphi}}_\ell \tag{14}$$

This article has been accepted for publication in a future issue of this journal, but has not been fully edited. Content may change prior to final publication. Citation information: DOI 10.1109/TPWRD.2020.3033755, IEEE Transactions on Power Delivery

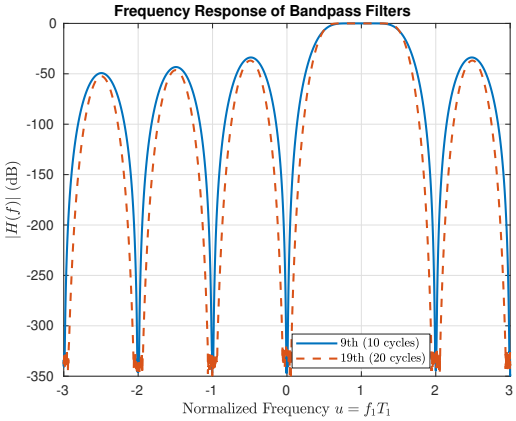

Fig. 3. Frequency response of nonic and decimononic bandpass filters.

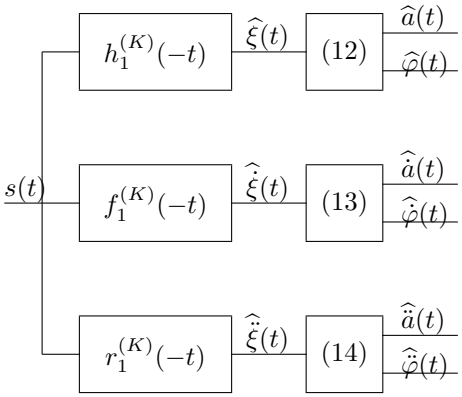

Fig. 4. Flowchart of the proposed method. First, the signal $s(t)$ is filtered by the bandpass filters $h_1^{(K)}(-t)$, $f_1^{(K)}(-t)$, and $r_1^{(K)}(-t)$ to produce estimates of the complex phasor, and its first two derivatives. Then, equations (12)-(14) are applied to obtain amplitude and phase derivatives at the output.

where $\widehat{a}_\ell$ and $\widehat{\varphi}_\ell$ are the estimated amplitude and phase, respectively, and their derivatives are indicated with the corresponding number of dots. Notice that $\widehat{p}_\ell = \widehat{a}_\ell e^{j\widehat{\varphi}_\ell}$. In Appendix B is the code in Matlab to obtain those derivatives for $K > 3$.

Finally, Fig. 3 exhibits the frequency response in dB of the bandpass filters built with nonic and decimononic O-splines. Note they are very similar, with the first sidelobe at -33dB and stopbands going down to -350dB about the harmonic frequencies. The main difference of the decimononic filter is a wider stopband. This explains why their phasor estimates are very similar for the given signals. We use the nonic filter because its shorter length.

III. Obtaining the Synchrophasor from Real Signals

Fig. 4 illustrates the block diagram of the signal processing proposed in this paper. The first three blocks enclose the bandpass filters which obtain the phasor estimate $\widehat{\xi}(t)$ and its derivatives $\widehat{\dot{\xi}}(t)$, and $\widehat{\ddot{\xi}}(t)$, from which amplitude and phase derivatives are obtained by applying (12)-(14).

The key idea of this paper can be clearly seen in this diagram. Since O-splines converge to the $Sinc$ function as the order $K \to \infty$, their spectra converge to the rectangular spectrum of the ideal lowpass filter. Since the O-spline sequence is convergent in a metric space, then it is also a Cauchy sequence [34]. Therefore, it is sufficient to define any positive real number $\epsilon > 0$ to ensure that there is a positive integer N such that the (Euclidian) distance between two O-splines $d(\widetilde{\varphi}_0^{(n)}(t), \widetilde{\varphi}_0^{(m)}(t)) < \epsilon$, whenever $n, m > N$. We claim that with $N = 9$ the distance is already sufficiently small, and so does the distance between the estimated phasors. In consequence, by increasing the order K of the filters $h_1^{(K)}(t)$, $f_1^{(K)}(t)$, and $r_1^{(K)}(t)$, the estimates of amplitude and phase (and derivatives), will converge to the ideal ones.

We do not recommend to modify this scheme with the differentiators suggested by the Standard, since the differentiators obtained by applying those short difference equations to the discrete version of the O-spline $\widetilde{\varphi}_0^{(K)}(u)$ are not equal to those of $\widetilde{\dot{\varphi}}_0^{(K)}(u)$ and $\widetilde{\ddot{\varphi}}_0^{(K)}(u)$, especially the second one, which has sharp spikes at its knots, where samples of two different polynomials are together.

IV. O-spline Compliance with the Synchrophasor Standard

After knowing how to obtain the O-splines, and how to design FIR filters, the first question we need to answer is if the nonic DTTFT filter complies the Synchrophasor Standard [10] and its first Amendment [11]. The answer is yes, its maximum errors are well below the benchmarks of the standard, as it was expected. In which follows, the error bounds achieved by the filter are listed case by case and compared with the boundaries of the standard [10]-[11] at the right. Since the support of the nonic O-spline is ten cycles, the nonic DTTFT filter is Class M.

A. Steady-State compliance

Measurements taken from steady-state signals with a frequency range of ± 5 Hz, and with harmonic distortion, are shown in the first two rows of Table I. As can be seen, the proposed filter is well below the limits in these cases.

The third row of Table I indicates the out-of-band test. The passband of the lowpass filter at -20dB is of 37Hz, which corresponds to a reporting rate of 74 frames per second. Since this is not admitted in the Standard, we take the reporting rate of 120. Thus, the frequency range of the input signal is 60 ± 12 Hz, with an outband frequency of 120Hz. Within this range, frequency and ROCOF are compliant, but TVE surpasses the limit of 1.3 %. TVE is compliant within the range of 60 ± 10 Hz.

B. Dynamic complience - Measurement Bandwidth and Ramp of System Frequency

The measurements for the amplitude and phase modulated signals, as well as the signal with a ramp rate of 1 Hz/s, and

This article has been accepted for publication in a future issue of this journal, but has not been fully edited. Content may change prior to final publication. Citation information: DOI 10.1109/TPWRD.2020.3033755, IEEE Transactions on Power Delivery

in the ± 5 Hz interval, are pointed out in Table II. The filter performance is remarkable for these signals.

C. Dynamic complience - Step Changes in Amplitude and Phase

Finally, the measurements of signals with amplitude or phase steps are shown in Table III. It passes all the tests, except the response time, which exceeds by 0.23 cycles the limit of the Standard, which is measured under ± 1 % of TVE. However the transient (from the steady-state end to the next steady-state start) is of 6 cycles for both steps.

TABLE I
STEADY STATE COMPLIENCE.

Case	Measurement	Standard Limit
$f_0 \pm 5$ Hz	$TVE = 2.185 \times 10^{-5}$ % $\|FE\| = 0$ Hz $\|RFE\| = 5.128 \times 10^{-6}$ Hz/s	1% 0.005 Hz 0.1 Hz/s
10 % Harmonic distortion up to 50th	$TVE = 2.5 \times 10^{-12}$ % $\|FE\| = 6 \times 10^{-15}$ Hz $\|RFE\| = 1.5 \times 10^{-13}$ Hz/s	1 % 0.025Hz Limit Suspended
Out-of-Band	$TVE = 2.9933$ % $\|FE\| = 1.166 \times 10^{-05}$ Hz $\|RFE\| = 6.9919 \times 10^{-05}$ Hz/s	1.3 % 0.01 Hz Limit Suspended

TABLE II
DYNAMIC COMPLIENCE - MEASUREMENT BANDWIDTH.

Case	Measurement	Standard Limit
Amplitude Modulated	$TVE \leq 2.5 \times 10^{-6}$ % $\|FE\| \leq 1.95 \times 10^{-7}$ Hz $\|RFE\| < 7.357 \times 10^{-6}$ Hz/s	3 % 0.3 Hz 14 Hz/s
Phase Modulated	$TVE \leq 4.71 \times 10^{-5}$ % $\|FE\| \leq 6.92 \times 10^{-6}$ Hz $\|RFE\| < 1.65 \times 10^{-3}$ Hz/s	3 % 0.3 Hz 14 Hz/s.
Frequency Modulated	$TVE \leq 2 \times 10^{-5}$ % $\|FE\| \leq 1.627 \times 10^{-6}$ Hz $\|RFE\| < 5 \times 10^{-4}$ Hz/s	1 % 0.01 Hz 0.2 Hz/s

TABLE III
DYNAMIC COMPLIENCE - STEP RESPONSES.

Case	Measurement	Standard Limit
Amplitude Step	Response time = 7.23 cycles delay time = 0 cycles Overshoot = 6.4 % Frequency response time = 6 cycles ROCOF response time = 6 cycles	7 cycles $\frac{1}{4}$ cycle 10 % 14 cycles 14 cycles
Phase Step	Response time = 7.37 cycles delay time = 0 cycles Overshoot = 7.4 % Frequency response time = 6 cycles ROCOF response time = 8 cycles	7 cycles $\frac{1}{4}$ cycle 10 % 14 cycles 14 cycles
Modulated Frequency	$TVE \leq 2 \times 10^{-5}$ % $\|FE\| \leq 1.627 \times 10^{-6}$ Hz $\|RFE\| < 5 \times 10^{-4}$ Hz/s	1 % 0.01 Hz 0.2 Hz/s

V. STUDY CASE: EVENT IN SYSTEM WITH SOLAR AND WIND POWER GENERATION

The topology of the low-voltage distributed generation system analyzed in this paper is displayed in Fig. 5 and

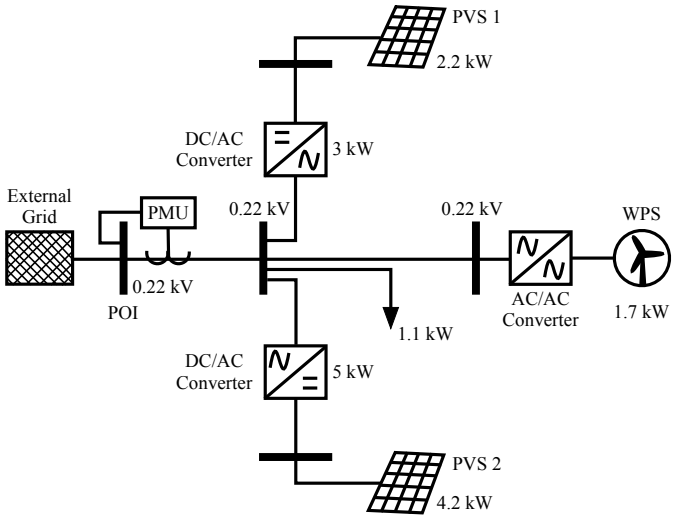

Fig. 5. Topology of the low-voltage distributed generation system considered in this paper with two PVSs and one WPS interconnected to the grid.

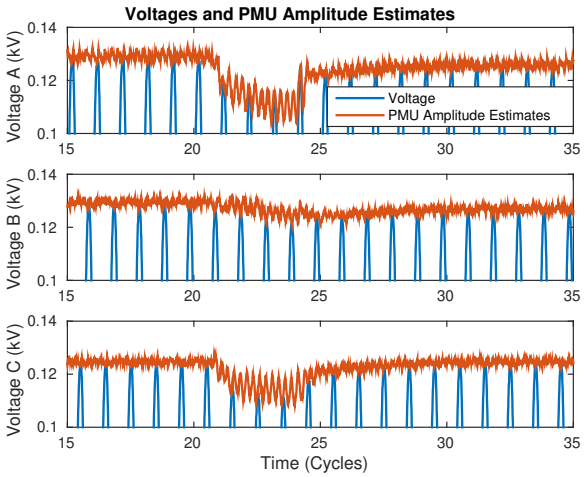

Fig. 6. Voltage waveforms with amplitude estimated by the PMU.

described in the following. Installed power of 8.1 KW with two photovoltaic systems (PVS) and one wind power system (WPS). Most of the time, the PVS is exposed to 12 sun hours, which is sometimes affected by unclear sky associated with cloudy conditions, changing the generated power, and causing abrupt current drops or variations on electrical variables monitored in the point of interconnection (POI), or point of common coupling toward the low-voltage power grid. Similarly, generated power by the WPS depends on the total power available in the wind (this is a function of air density, wind speed, and the area swept by the blades) [35].

The system is monitored using a PMU equipped with the Cosine filter phasor estimator, which carries out the estimation process from voltage and current signals in the *abc* reference frame, and in their symmetrical components. Three transformers are employed to transduce the current inputs toward the PMU. Signals are sampled at 128 samples per fundamental cycle corresponding to 60 Hz.

A sudden change in the system frequency triggered the

This article has been accepted for publication in a future issue of this journal, but has not been fully edited. Content may change prior to final publication. Citation information: DOI 10.1109/TPWRD.2020.3033755, IEEE Transactions on Power Delivery

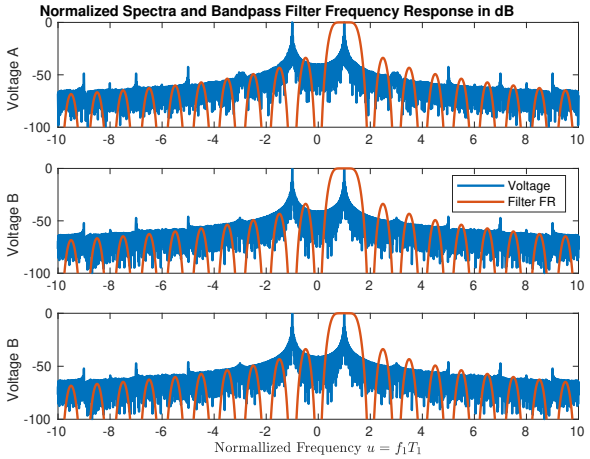

(a) Spectra and fundamental bandpass filter

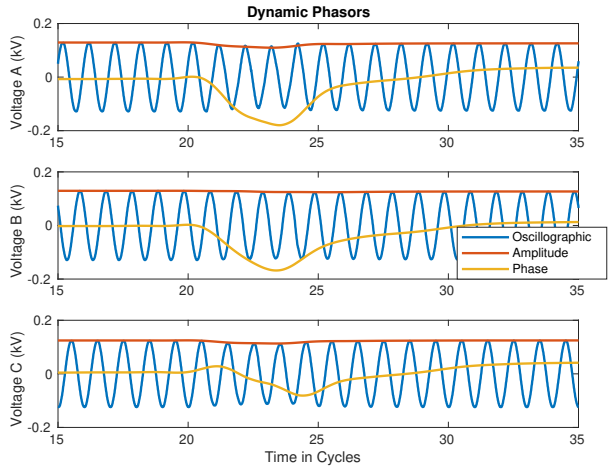

(b) Dynamic Phasors.

Fig. 7. Voltage spectra and frequency response of the (nonic DTTFT) filter. At the bottom, voltage oscillography and the corresponding synchrophasors (amplitude and phase). Phases are forced to start at zero.

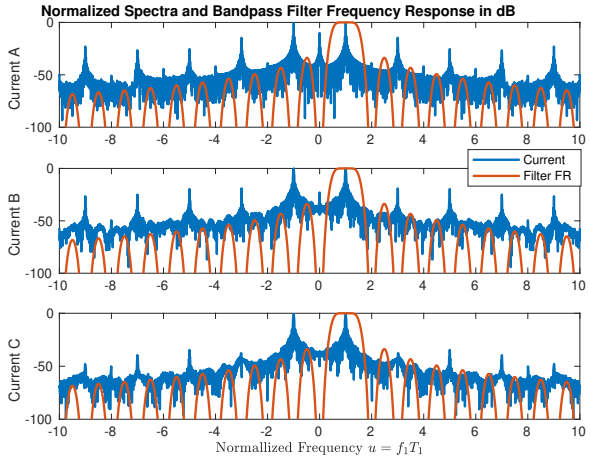

(a) Spectra and fundamental bandpass filter

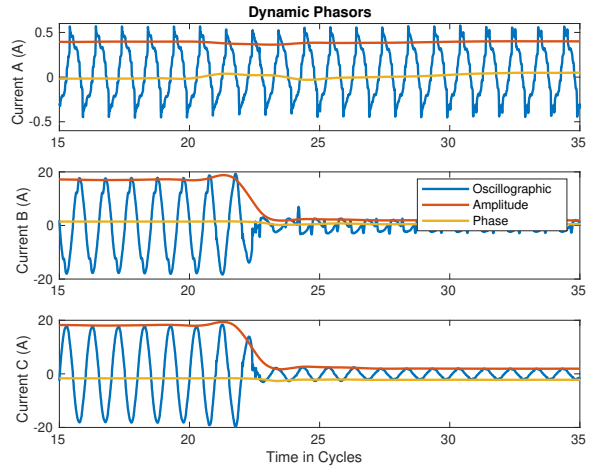

(b) Dynamic Phasors.

Fig. 8. Current spectra and frequency response of the (nonic DTTFT) filter. At the bottom, current oscillography and the corresponding synchrophasors (amplitude and phase).

recording of the event. The instantaneous measurements of voltages, together with their PMU amplitude estimates are illustrated in Fig. 6. Note that amplitude estimates have a significant quivering behavior, especially in voltage. The amplitude estimates of currents are similar than those of the voltages. This erratic behavior in the PMU amplitude estimates was not found in those obtained from the oscillographic data with our implemented Cosine filter, which is supposedly applied in the PMU. PMU phase estimates are even more erratic than those of amplitude.

VI. Dynamic Phasor of Oscillographic Signals

In this section, the synchrophasors of voltage and currents obtained with a nonic DTTFT are illustrated.

The top plot of Fig. 7 shows the spectra of voltage signals with the frequency response of the nonic DTTFT filter (in dB). For the given signals, it performs as an ideal filter, i. e., with a flat top unit gain about the fundamental frequency, and zero gain stopbands (going down to -350 dBs) about harmonic frequencies, where the predominant non-fundamental energy of the signals is found. This is important especially in the currents which are shown in the top plot of Fig. 8. The module and phase angle of the estimated synchrophasors obtained from the oscillographic data are shown at the bottom. Those plots are focused on the interval with the stronger dynamic changes. By comparing the oscillographic data with the reconstructed signal with the synchrophasor in Fig. 9, it can be seen that the nonic DTTFT filter makes an excellent rejection of the apparent harmonic components in the top plot of Fig. 8, and preserving the fundamental component with high fidelity due to its wide flat-top passband.

A. TVE of Voltages and Currents

Current phasor estimates are shown in Fig. 10. The left column of those figures depicts the amplitude, and the right one the phase angle. Nonic DTTFT estimates are superposed of those of the PMU. Notice the PMU phase estimates are worst than those of amplitude, for example, those of Ia have

This article has been accepted for publication in a future issue of this journal, but has not been fully edited. Content may change prior to final publication. Citation information: DOI 10.1109/TPWRD.2020.3033755, IEEE Transactions on Power Delivery

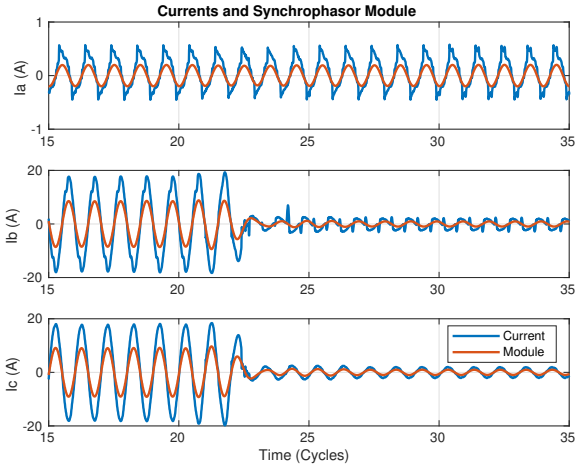

Fig. 9. Currents and their synchrophasor synthetic signals.

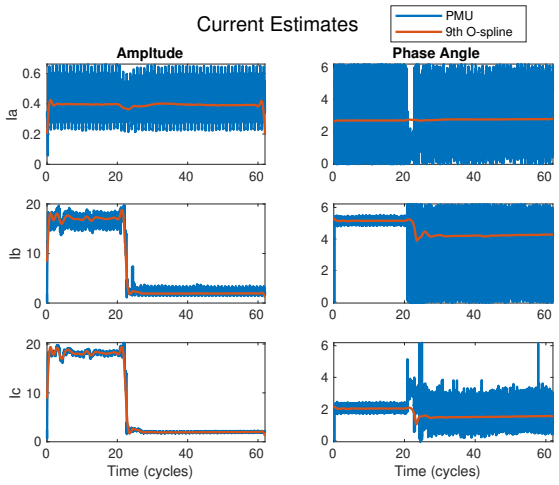

Fig. 10. Current phasor estimates. At the left column the amplitudes, and at the right column the corresponding phase angles.

the full range from 0 to 2π. The same can be said about the phase estimates of the voltage signals.

This erratic behavior in the PMU amplitude and phase estimates is maybe due to a random variation in the sampling time observed in the time variable reported by the PMU.

Fig. 11 shows the TVE of the PMU estimates. TVE is calculated with the synchrophasor obtained with the nonic O-spline filter from the voltage and current oscillographic data of the PMU. As can be seen, the PMU performance is very poor, since its estimates have a TVE range in the hundreds.

B. Frequency and ROCOF Estimates

Finally, the top plot of Fig. 12 depicts the frequencies obtained from voltages with the nonic O-spline first differentiator, and at the bottom the ROCOF obtained with the second one. Both estimates are calculated according to (13)-(14). Since voltage phase estimates are continuous and smooth (see the bottom plot of Fig. 7), their derivative estimates are valid measurements. Notice that they are very clean as

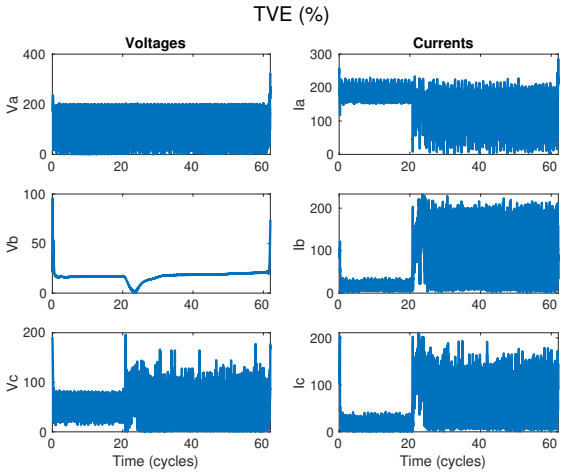

Fig. 11. TVE of PMU Voltage (left), and current (right) estimates.

compared with the noisy frequency estimates provided by most of the PMUs. Zero crossings of the ROCOF plots coincide with the *maxima* and *minima* in the frequency plots. Frequency estimates are compared with those rendered by the PMU. There is no information available about the algorithm employed by the PMU, but it can be seen that they correspond to per-segment averages, and delayed versions of its original frequency estimates. The average operator serves to clean its erratic behavior. In consequence, the frequency O-spline estimates are much less inexact than those provided by the PMU.

VII. Discussion

Nowadays, the estimation performance of PMUs can be only known through the benchmark signals of the standard, for which their synchrophasors are known. A ranked sequence of FIR filters that converges to the ideal filter is proposed in [24] . From that sequence, this paper chooses the lower rank filter that provides synchrophasor estimates sufficiently close

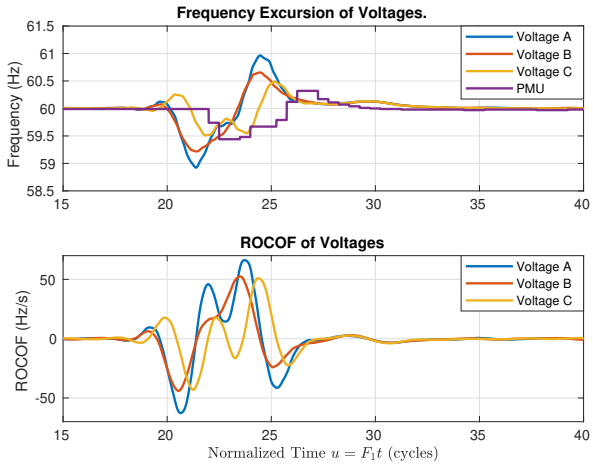

Fig. 12. Frequency and ROCOF estimates from voltage channels obtained with the nonic O-spline first and second differentiators.

to those obtained from real signals with the ideal filter. In this way, it opens the way to assess the accuracy of PMU results obtained with field signals. In our event, a nonic O-spline reaches an approximation very close to that of the decimononic one, but with a duration of only ten cycles. This duration is not large compared with the sixty cycles available in the oscillographic data, especially for the off-line comparative evaluation. The performance of this filter is better than those in [27], [28], and [29].

The applied method is done off-line. But the proposed filter can also be applied on-line, in applications allowing its length. This method must be accompanied by a spectral analysis to check that input signals do not have energy under the filter transition bands, as shown in the top plots of Figs. 7 and 8.

The computational complexity of the proposed method is very low ($\mathcal{O}(3N_0)$), since it consists in the implementation of three FIR filters, and Eqs. (12)-(14) that could be easily implemented even in a real PMU. In fact, it has been already implemented in its classical form in [36].

Finally, the proposed method could contribute to a more universal approach than the one defined in the Standard, that until now has limits defined by consensus that seem to endorse the lower order algorithms.

VIII. Conclusion

The paper proposes a quantitative method to assess the estimation performance of PMUs using signals from the field, such as those produced in a substation, and available in a control center, instead of employing only the few benchmark signals of the Standard. Real signals contain realistic harmonics and real noisy conditions as those shown in this paper. The attained results in the analyzed case exhibit very poor PMU estimates, since they are very erratic in both phase and amplitude, with intolerable TVEs with hundreds of times the tolerated ones. But the important contribution of this work is that it opens up the possibility of employing the TVE to assess and compare the estimation performance of different PMUs at a control center, when they monitor the same disturbance, today an unthinkable application.

Appendix A
MatLab Function to obtain the samples of the Kth O-spline and its First two Derivatives with N_0 Samples per Cycle.

```
function [phi,phip,phipp]=Osplinepp(K,N0)
%Order K>3
%N0 Number of samples per cycle
delt=1/N0;
unit=(0:delt:1-delt)';
knots=[flip(-[1:K]) [1:K]];
P=ones(N0,K+1); Pp=ones(N0,K+1);
Ppp=ones(N0,K+1);
ir0=0;
for nint=1:K+1
u=-(K+1)/2-1+nint+unit;
coef= [1, -knots(ir0+1)]/(-knots(ir0+1));
for k=1:K
P(:,nint)=P(:,nint).*(u-knots(ir0+k))/...
(-knots(ir0+k));
if k>1 coef = conv(coef, [1, -knots(ir0+k)]/...
(-knots(ir0+k))); end;
end;
%Derivative Polynomial coefficients
C(:,nint)=coef'; Cp(:,nint)=polyder(coef)';
Cpp(:,nint)=polyder(Cp(:,nint))';
%First derivative by Horner scheme
Pp(:,nint)=Cp(1,nint)*Pp(:,nint);
for k=1:K-1
Pp(:,nint)=Pp(:,nint).*u + Cp(k+1,nint);
end;
%Second derivative by Horner scheme
Ppp(:,nint)=Cpp(1,nint)*Ppp(:,nint);
for k=1:K-2
Ppp(:,nint)=Ppp(:,nint).*u + Cpp(k+1,nint);
end;
ir0=ir0+1;
end;
N=(K+1)*N0;
phi=reshape(P,[N,1]); phip=reshape(Pp,[N,1]);
phipp=reshape(Ppp,[N,1]);
```

Appendix B
State Estimator

```
hm=phi/N0.*exp(j*2*pi/N0*n);
hpm=F0*phip/N0.*exp(j*2*pi/N0*n);;
hppm=F0^2*phipp/N0.*exp(j*2*pi/N0*n);
%%%%%%%%%%%%%%%%%%%%%%%%%%%%%%%%%%%%%%%%%%%%
function [a,p,ap,pp,app,ppp]=...
statestimator(hm,hpm,hppm,s)
%hm,hpm,hppm impulse response of the
%FIR filter and first two derivatives
%sh samples of the filtered signal
%%%%%%%%%%%%%%%%%%%%%%%%%%%%%%%%%%%%%%%%%%%%
%a,p       amplitude and phase
%ap,pp     first derivatives of a and p
%app,ppp   second derivvatives of a and p
%%%%%%%%%%%%%%%%%%%%%%%%%%%%%%%%%%%%%%%%%%%%
%Amplitude and Phase estimation
k=(0:Nc*N0-1)'; p=conv(s, hm,'same');
ah=abs(p); ph=angle(p);   % rotating phase
phc=angle(p.*exp(-2j*pi/N0*k));% antirotated
a=2*ah; p=phc;
%%%%%%%%%%%%%%%%%%%%%%%%%%%%%%%%%%%%%%%%%%%%
%Frequency estimation
pp=conv(s,hpm,'same');
ppc=pp.*exp(-j*ph);
ahp=real(ppc);
php=imag(ppc)./ah;
ap=ahp; pp=php/(2*pi); %frequency deviation
%%%%%%%%%%%%%%%%%%%%%%%%%%%%%%%%%%%%%%%%%%%%
%ROCOF Estimation
ppp=conv(s,hppm,'same');
pppc=ppp.*exp(-j*ph);
ahpp=real(pppc)+ah.*php.^2;
```

```
phpp=( imag(pppc)- 2*ahp.*php )./ah;
app=ahpp; ppp=phpp/(2*pi);
%%%%%%%%%%%%%%%%%%%%%%%%%%%%%%%%%%%%%%%%%%%%
```

REFERENCES

[1] R. Gore and M. Kande, "Analysis of wide area monitoring system architectures," in *2015 IEEE International Conference on Industrial Technology (ICIT)*, March 2015, pp. 1269–1274.

[2] P. Overholt, D. Ortiz, and A. Silverstein, "Synchrophasor technology and the DOE: Exciting opportunities lie ahead in development and deployment," *IEEE Power Energy Mag.*, vol. 13, no. 5, pp. 14–17, Sept 2015.

[3] DOE, "Smart grid investment grant program - progress report," US Department of Energy, Tech. Rep., 2012.

[4] R. M. Moraes, H. A. R. Volskis, and Y. Hu, "Deploying a large-scale pmu system for the brazilian interconnected power system," in *2008 Third International Conference on Electric Utility Deregulation and Restructuring and Power Technologies*, April 2008, pp. 143–149.

[5] R. B. Sharma and G. M. Dhole, "Synchrophasor measurement network and its applications in indian grid," in *2016 International Conference on Emerging Trends in Electrical Electronics Sustainable Energy Systems (ICETEESES)*, March 2016, pp. 30–34.

[6] J. Y. Yanshan Yu and B. Chen, "The smart grids in China - A review," *Energies*, vol. 5, pp. 1321–1338, 2012.

[7] Z. Huang, B. Kasztenny, V. Madani, K. Martin, S. Meliopoulos, D. Novosel, and J. Stenbakken, "Performance evaluation of phasor measurement systems," in *2008 IEEE Power and Energy Society General Meeting*, July 2008, pp. 1–7.

[8] J. A. de la O Serna, "Dynamic phasor estimates for power system oscillations," *IEEE Trans. Instrum. Meas.*, vol. 56, no. 5, pp. 1648–1657, Oct 2007.

[9] "IEEE/IEC International Standard - Measuring relays and protection equipment - part 118-1: Synchrophasor for power systems - Measurements," *IEC/IEEE 60255-118-1:2018*, pp. 1–78, Dec 2018.

[10] "IEEE Standard for Synchrophasor Measurements for Power Systems," *IEEE Std C37.118.1-2011 (Revision of IEEE Std C37.118-2005)*, pp. 1–61, Dec 2011.

[11] "IEEE standard for synchrophasor measurements for power systems – amendment 1: Modification of selected performance requirements," *IEEE Std C37.118.1a-2014 (Amendment to IEEE Std C37.118.1-2011)*, pp. 1–25, 2014.

[12] A. G. Phadke and T. Bi, "Phasor measurement units, WAMS, and their applications in protection and control of power systems," *Journal of Modern Power Systems and Clean Energy*, vol. 6, no. 4, pp. 619–629, Jul 2018. [Online]. Available: https://doi.org/10.1007/s40565-018-0423-3

[13] A. G. Phadke, J. S. Thorp, and M. G. Adamiak, "A new measurement technique for tracking voltage phasors, local system frequency, and rate of change of frequency," *IEEE Trans. Power App. Syst.*, vol. PAS-102, no. 5, pp. 1025–1038, May 1983.

[14] J. Sykes, K. Koellner, W. Premerlani, B. Kasztenny, and M. Adamiak, "Synchrophasors: A primer and practical applications," in *2007 Power Systems Conference*, March 2007, pp. 213–240.

[15] D. Macii, D. Petri, and A. Zorat, "Accuracy analysis and enhancement of dft-based synchrophasor estimators in off-nominal conditions," *IEEE Trans. Instrum. Meas.*, vol. 61, no. 10, pp. 2653–2664, Oct 2012.

[16] M. R. D. Zadeh and Z. Zhang, "A new dft-based current phasor estimation for numerical protective relaying," *IEEE Trans. Power Del.*, vol. 28, no. 4, pp. 2172–2179, Oct 2013.

[17] J. A. de la O Serna, "Analyzing power oscillating signals with the O-splines of the Discrete Taylor-Fourier Transform," *IEEE Trans. Power Syst.*, vol. 33, no. 6, pp. 7087–7095, Nov 2018.

[18] J. A. de la O Serna and J. Rodriguez-Maldonado, "Taylor-kalman-fourier filters for instantaneous oscillating phasor and harmonic estimates," *IEEE Trans. Instrum. Meas.*, vol. 61, no. 4, pp. 941–951, April 2012.

[19] P. Castello, M. Lixia, C. Muscas, and P. A. Pegoraro, "Impact of the model on the accuracy of synchrophasor measurement," *IEEE Trans. Instrum. Meas.*, vol. 61, no. 8, pp. 2179–2188, Aug 2012.

[20] R. Ghiga, K. Martin, Q. Wu, and A. Nielsen, "Phasor measurement unit test under interference conditions," *IEEE Trans. Power Del.*, vol. PP, no. 99, pp. 1–1, 2017.

[21] D. Petri, D. Fontanelli, D. Macii, and D. Belega, "A dft-based synchrophasor, frequency and rocof estimation algorithm," in *2013 IEEE International Workshop on Applied Measurements for Power Systems (AMPS)*, Sept 2013, pp. 85–90.

[22] A. J. Roscoe, G. M. Burt, and G. Rietveld, "Improving frequency and rocof accuracy during faults, for p class phasor measurement units," in *2013 IEEE International Workshop on Applied Measurements for Power Systems (AMPS)*, Sept 2013, pp. 97–102.

[23] D. Macii, D. Fontanelli, D. Petri, and G. Barchi, "Impact of wideband noise on synchrophasor, frequency and rocof estimation," in *2015 IEEE International Workshop on Applied Measurements for Power Systems (AMPS)*, Sept 2015, pp. 43–48.

[24] J. A. de la O Serna, "Dynamic harmonic analysis with FIR filters designed with O-splines," *IEEE Trans. Circuits Syst. I*, in press, DOI 10.1109/TCSI.2020.2996976.

[25] R. M. Moraes, Y. Hu, G. Stenbakken, K. Martin, J. E. R. Alves, A. G. Phadke, H. A. R. Volskis, and V. Centeno, "PMU interoperability, steady-state and dynamic performance tests," *IEEE Trans. Smart Grid*, vol. 3, no. 4, pp. 1660–1669, 2012.

[26] T. Trummal, J. Kilter, M. Loper, and I. Palu, "Phasor measurement units performance assessment during power system disturbances using real-time digital simulator," in *2019 Electric Power Quality and Supply Reliability Conference (PQ) 2019*, 2019, pp. 1–8.

[27] K. Duda, T. P. Zielinski, A. Bien, and S. H. Barczentewicz, "Harmonic phasor estimation with flat-top fir filter," *IEEE Trans. Instrum. Meas.*, vol. 69, no. 5, pp. 2039–2047, 2020.

[28] S. Xu, H. Liu, T. Bi, and K. E. Martin, "A high-accuracy phasor estimation algorithm for PMU calibration and its hardware implementation," *IEEE Trans. Smart Grid*, vol. 11, no. 4, pp. 3372–3383, 2020.

[29] P. Castello, J. Liu, C. Muscas, P. A. Pegoraro, F. Ponci, and A. Monti, "A fast and accurate pmu algorithm for p+m class measurement of synchrophasor and frequency," *IEEE Trans. Instrum. Meas.*, vol. 63, no. 12, pp. 2837–2845, 2014.

[30] G. Benmouyal and K. Zimmerman, "Experience with subcycle operating time distance elements in transmission line digital relays," in *37th Annual Western Protective Relay Conference*, 2010, pp. 1–12.

[31] A. G. Phadke and J. S. Thorp, *Synchronized phasor measurements and their applications*. Springer, 2008, vol. 1.

[32] J. G. Proakis and D. G. Manolakis, *Digital Signal Processing: Principles, Algorithms, and Applications*, 4th ed. Prentice Hall, 2006.

[33] J. A. De la O Serna, "Synchrophasor measurement with polynomial phase-locked-loop Taylor-Fourier filters," *IEEE Trans. Instrum. Meas.*, vol. 64, no. 2, pp. 328–337, 2015. [Online]. Available: http://dx.doi.org/10.1109/TIM.2014.2344333

[34] M. Rosenlicht, *Introduction to Analysis*, dover, New York, 1968.

[35] J. F. Manwell, J. G. McGowan, and A. L. Rogers, *Wind energy explained: theory, design and application*. John Wiley & Sons, 2010.

[36] M. R. A. Paternina, J. M. Ramirez, and A. Z. Mendez, "Real-time implementation of the digital Taylor-Fourier transform for identifying low frequency oscillations," *Electric Power Systems Research*, vol. 140, pp. 846 – 853, 2016. [Online]. Available: http://www.sciencedirect.com/science/article/pii/S0378779616301389

José Antonio de la O Serna (SM'03) was born in San Pedro, Coahuila, Mexico, in 1953. He received the Ph.D. degree from Telecom ParisTech, Paris, France, in 1982. He was a Professor with Monterrey Institute of Technology, Monterrey, from 1982 to 1986. From 1988 to 1993, he was with the Department of Electrical Engineering, Polytechnic School, Yaounde, Cameroon. He was a member of the Doctoral Committee with UANL, where he is currently a Research Professor. Dr. de la O Serna is a member of the Mexican Research System.

Mario Arrieta Paternina (M'11) B.S. and M.Sc. in Electrical Engineering from the National University of Colombia, in 2007 and 2009, respectively. In 2017, he obtained his Ph.D. degree in electrical engineering from CINVESTAV. He joined the Department of Electrical Engineering, UNAM, in 2017. He was a visiting scholar at Rensselaer Polytechnic Institute in 2016. His areas of interest include dynamic equivalents, coherency, modal identification, and model reduction of power systems.

Alejandro Zamora-Mendez (M'12) obtained his B.S. and M.Sc. in Electrical Engineering from Universidad Michoacana de San Nicolas de Hidalgo (UMSNH), Morelia, Mexico, in 2005 and 2008, respectively. In 2016, he obtained his Ph.D. degree in electrical engineering from CINVESTAV. He joined the Electrical Engineering Faculty, UMSNH, in 2008, where he is a full-time Professor. He was a visiting scholar at Washington State University in 2015. His areas of interest are in operation and control of power systems.